Blood First Edition Paper, prepublished online October 17, 2018; DOI 10.1182/blood-2018-05-850321

Murine myeloproliferative disorder as a consequence of impaired collaboration between dendritic cells and CD4 T cells

Running title: Defective DC-T cell communication leads to MPD

Stéphanie Humblet-Baron[1,2*], John S. Barber[1,2*], Carlos Roca[1,2], Aurelie Lenaerts[1,2], Pandelakis A. Koni[3] and Adrian Liston[1,2^]

[1] VIB Center for Brain & Disease Research, Leuven, Belgium
[2] KU Leuven - University of Leuven, Department of Microbiology and Immunology, Leuven, Belgium.
[3] Georgia Cancer Center, Augusta University, Georgia, USA.

* these authors contributed equally
^ correspondence to adrian.liston@vib.be

Key points: Myeloproliferation can result of defects in DC-CD4 T cell interactions as well as from numerical deficits in DCs

Dendritic cells (DCs) are a key cell type in the initiation of the adaptive immune response. Recently an additional role for DCs in suppressing myeloproliferation was discovered. Myeloproliferative disorder (MPD) was observed in both murine studies with constitutive depletion of DCs, and in patients with congenital deficiency in DCs caused by mutations in *GATA2* or *IRF8*. The mechanistic link between DC deficiency and MPD was not predicted through the known biology and has remained an enigma. Prevailing models suggest numerical DC deficiency leads to MPD through compensatory myeloid differentiation. Here we formally tested whether MPD can also arise through a loss of DC function without numerical deficiency. Using mice where DCs are deficient in antigen presentation, we find spontaneous myeloproliferative disorder characterized by splenomegaly, neutrophilia and extramedullary hematopoiesis, despite normal numbers of DCs. Disease development was dependent on loss of the MHC class II antigen presenting complex on DCs and was eliminated in mice deficient in total lymphocytes. Mice lacking both MHCII and CD4 T cells did not develop disease. MPD was thus paradoxically contingent on both the presence of CD4 T cells and on a failure of DCs to activate CD4 T cells, trapping the cells in a naïve Flt3L-expressing state. These results identify a novel requirement for intercellular collaboration between dendritic cells and CD4 T cells to regulate myeloid differentiation. Our findings support a new conceptual framework of DC biology in preventing MPD in mice and humans.

Introduction

Dendritic cells (DCs) are specialized antigen-presenting cells that play a crucial role in coordinating innate and adaptive immune responses. They are primarily recognized for their T cell priming capacities, both in the periphery, where they direct responses against infections [1], and in the thymus, where they play an important role in negative selection [2–4] and induction of regulatory T cells[5]. Given these functions, it is unsurprising that dendritic cell ablation or deficiency leads to susceptibility to infection and autoimmunity [6–10]. A more perplexing manifestation resulting from dendritic cell deficiency, in both mice and humans, is the development of a spontaneous myeloproliferative disorder (MPD). The connection between DC biology and the regulation of myeloid homeostasis has remained an enigma.

MPD in the setting of DC deficiency was first characterized in mice by two groups contemporaneously where mice expressing diphtheria toxin (DT) fragment A in the Rosa locus were crossed with the CD11c-Cre mice [11,12]. One group reported susceptibility to murine viral infections, variable alterations in T cell subsets, and a form of MPD characterized by monocytic and neutrophilic expansion [11], while the other described spontaneous autoimmunity and significant neutrophilia [12]. Subsequently, similar MPD phenotypes or significant neutrophilia have been described in other mouse models of DC deficiency, including IRF8 deficiency [13,14], TAK1 conditional deficiency in CD11c+ cells [15], pan-hematopoietic Cbfβ deficiency [8] and zDC-DTR mice [16]. In parallel, clinical analysis of patients with monogenic DC deficiency, such as GATA2 and IRF8 deficiency, has identified similar myeloproliferative and myelodysplastic disorders[7,17–19]. While the manifold impact of mutations in *GATA2* and *IRF8* may be driving pleiotropic effects with distinct mechanistic pathways driving DC deficiency and MPD, the replication of the phenotype in DC-depleted mice indicates that a conserved causal relationship underlies these conditions.

The prevailing model to explain the mechanistic link between DC deficiency and MPD is one of differentiation niches, whereby the void left by absent DCs results in an excess of growth factors or stimuli that drive myeloid precursor cells into a pathogenic state. However, an alternative hypothesis, that MPD is a direct consequence of a lack of DC function (akin to susceptibility to infection and autoimmunity) has not been formally ruled out. Here, we test whether functional DC deficiency also leads to myeloproliferation using mice in which DCs are present but deficient in antigen presentation function. Mice with DCs deficient for MHCII developed MPD with splenomegaly, neutrophilia, and extramedullary hematopoiesis. Surprisingly, crossing these mice to a Rag^{KO} background rescued the phenotype, with CD4 T cells required for disease manifestation. Naïve antigen-inexperienced CD4 T cells expressed higher levels of Flt3L, providing a mechanistic insight into the requirement for intercellular collaboration between dendritic cells and CD4 T cells to regulate myeloid differentiation and prevent MPD.

Materials and Methods

Mice

$CD11c^{\Delta MHCII}$ mice were generated through the intercross of CD11c-Cre mice[20] and $MHCII^{flox}$ mice[21], both on the C57BL/6 background. "Wildtype" controls were Cre-negative $MHCII^{flox}$ littermates or regular C57BL/6 mice. The $CD11c^{\Delta MHCII}$ strain was further intercrossed with $Rag1^{KO}$ [22] and $\beta2m^{KO}$ [23] strains, to create the $Rag^{KO}CD11c^{\Delta MHCII}$ and $\beta2m^{KO}CD11c^{\Delta MHCII}$ strains, respectively. $MHCII^{KO}$ mice [24] were intercrossed to the C57BL/6 CD45.1 background. Mice were maintained in specific pathogen-free facilities of University of Leuven. All experiments were approved by the University of Leuven ethics committee.

Bone-marrow-derived dendritic cell culture

Single BM cell suspension were differentiated *in vitro* towards DCs for 8 days in RPMI 1640 medium (supplemented with 5% FBS, 10 mM HEPES, 100 U/ml penicillin, 100 µg/ml streptomycin,100x L-glu and 50 µM 2-ME) with the addition of 20 ng/ml of GM-CSF every 2 days (eBioscience/Thermo Fisher Scientific). Cells were plated in six-well plates at a density of 1 x 10^6 cells/ml and incubated at 37°C in humidified air with 5% CO2. On day 6, wells were harvested by vigorous washing and supernatant was transferred to a new plate to mature for an additional 48 hours without GM-CSF (differentiated plate). On day 8, both plates (undifferentiated and differentiated) were harvested and evaluated by flow cytometry.

Cell processing and flow cytometry

Spleen and lymph nodes were cut in small pieces and digested with collagenase D (0.5mg/ml) (Roche). Further single-cell suspensions were prepared from mouse thymus, bone marrow, spleen and lymph nodes. Single-cell suspensions were prepared from mouse thymus, bone marrow and spleen. All cells were fixed with BD Cytofix™ (BD, Biosciences) or fixed and permeabilized with the eBioscience Foxp3 staining kit (eBioscience/Thermo Fisher Scientific). For intracellular cytokine staining, lymphocytes were plated at 5x10^5 cells/well in 96-well tissue culture plates in complete RPMI containing phorbol myristate acetate (50 ng/mL; Sigma-Aldrich), ionomycin (250 ng/mL; Sigma-Aldrich) and Monensin (1/1500; BD, Bioscience) for 4 hours at 37°C. Anti-murine antibodies included anti-CD4 (RM4-5), anti-CD8α (53-6.7), anti-Foxp3 (FJK-16s), anti-CD44 (IM7), anti-CD62L (MEL-14), anti-Gr1 (RB6-8C5), anti-CD11b (M1/70), anti-Ly6C (HK1.4), anti-F4/80 (BM8), anti-CD11c (N418), anti-MHCII (M5/114.15.2), anti-CD86 (PO3.1), anti-B220 (RA3-6B2), anti-NK1.1 (PK136), anti-CD3 (145-2c11), anti-Sca1 (D7), anti-c-Kit (2B8), anti-PDCA1 (eBio927), anti-CD31 (390), anti-IL2 (JES6-5H4), anti-IFNγ

(XMG1.2), anti-IL4 (BVD6-24G2) and anti-IL17 (eBio17B7) all from (eBioscience/Thermo Fisher Scientific). Routine data analysis was performed with FlowJo (see **Figure S1** for representative gating).

Cluster analysis

The cluster analysis was performed with custom code written in R v. 3.4.4[25]. The starting data were the leukocytes identified by gating for non-debris, singlet events, maintaining the compensation and bi-exponential transformations applied. Event data from six samples were merged, resulting in a total number of approximately 10^6 cells, restricted to the markers CD11b, CD11c, Gr1, Ly6c, and F4/80. The package flowWorkspace v. 3.26.9[26] was used to import data in the R environment. Clusters were identified with FlowSOM v. 1.10.0[27] and ConsensusClusterPlus v. 1.42.0, using a predetermined number of 10 clusters and default configuration parameters. The t-SNE representation was obtained on a 10% random subsample, using Rtsne v. 0.13[28,29] with default parameters, except for an increase in convergence to 10,000 steps. Plots were prepared with ggplot2 v. 2.2.1[30] (Wickham, 2009) and RColorBrewer v. 1.1-2[31].

Histology

Mouse tissues were preserved in 10% formalin and processed into paraffin-embedded tissue blocks by Histology Consultation Services. Each block had thin (~4µm) sections cut on a microtome, mounted on glass slides, and stained with hematoxylin and eosin (H&E). Pathological diagnosis was performed by Biogenetics Research Laboratories.

qPCR assay

Single-cell suspensions were prepared from mouse spleen and lymph nodes. CD4+ T cells were enriched using MagniSort™ Mouse CD4 T cell Enrichment Kit (Thermo Fisher Scientific) before staining with anti-CD25 (PC61.5), anti-CD4 (GK1.5), anti-CD44 (IM7), anti-CD62L (MEL-14) all from (eBioscience/Thermo Fisher Scientific) before sorting naïve and memory populations on a FACSAria^{TM} I cytometer (BD Biosciences). Total RNA was isolated using TRIzol Reagent (Invitrogen/Thermo Fisher Scientific). Complementary DNA was synthesized from RNA using the GoScript Reserve Transcription System (Promega). Real-time quantitative PCR was performed using the Primetime qPCR assay (Integrated DNA Technologies) with gene-specific probes (Flt3L PT.58.5907613, Polr2a PT.39a.22214849) on a StepOnePlus real-time PCR system (Applied Biosystems,). Analysis was performed with the $2^{-\Delta\Delta CT}$ method, and quantifications were normalized to the housekeeping gene *Polr2a*. Experiments were performed with technical duplicates.

Statistical analyses

Single comparisons were analyzed using the non-parametric Mann-Whitney *U* test. Cumulative incidence curves were analyzed using a log-rank test. Multiple group comparisons were analyzed using one-way ANOVA followed by Tukey's multiple comparisons test. qPCR data was analyzed by an unpaired t test. All strain comparisons were run in parallel, with the baseline data on wildtype and CD11c$^{\Delta MHCII}$ mice repeated on Figures 4-6 to allow direct comparison across strains.

Results

Dendritic cell functional impairment drives myeloproliferative disease

In order to determine the mechanistic basis of the relationship between DC deficiency and MPD, we first sought to assess whether myeloproliferation, previously observed in numerical absence of DCs, can also occur with the loss of the antigen-presenting functions that DCs provide. We therefore generated CD11c$^{\Delta MHCII}$ mice to disrupt the key DC function of professional antigen presentation while maintaining normal DC numbers. CD11c$^{\Delta MHCII}$ mice appropriately lacked MHCII expression on the CD11c^{+} compartment **(Figure 1A**), while preserving normal splenic DC percentages within the classical DC compartments (**Figure 1B**). Absolute number of DCs was unchanged (**Figure S3A**). The plasmacytoid DC compartment also remained fairly similar at all time points, with a small decrease in the CD11c$^{\Delta MHCII}$ mice at one year old in comparison to wildtype animals (**Figure 1C**). Likewise, *in vitro* DC maturation was normal in CD11c$^{\Delta MHCII}$ mice (**Figure S2**). Despite no major differences in broad DC subsets in CD11c$^{\Delta MHCII}$ mice, we did observe a significant shift from CD8^{+} CD11b^{-} cDCs to CD8^{-}CD11b^{+} cDCs over time (**Figure S3B,C**), indicating secondary effects to impaired antigen presentation. These data support the use of CD11c$^{\Delta MHCII}$ mice as a system to study DC functional impairment without the induction of a numerical deficit. Having validated the CD11c$^{\Delta MHCII}$ system, we monitored the mice for signs of disease. CD11c$^{\Delta MHCII}$ mice developed normally, although total weight of CD11c$^{\Delta MHCII}$ mice decreased compared to wildtype mice over time (**Figure 1D**). CD11c$^{\Delta MHCII}$ mice developed splenomegaly as early as 12 weeks, with markedly increasing severity and incidence over time (**Figure 1E, F**). To investigate the origin of the splenomegaly in CD11c$^{\Delta MHCII}$ mice we first took a histological approach. Neither the spleens, nor other organs, showed any signs of lymphocytic infiltrate in CD11c$^{\Delta MHCII}$ mice, suggesting that splenomegaly was not secondary to autoimmune disease (**Figure S4**). However, both the spleen and liver demonstrated signs of extra-medullary hematopoiesis, with haematopoietic stem cells observed in both organs in CD11c^{MHCIIflox} mice (**Figure S4**). These data identify CD11c$^{\Delta MHCII}$ mice as potentially developing MPD, analogous to the DC-deficient models.

To test for MPD in CD11c$^{\Delta MHCII}$ mice, we used a myeloid-based staining panel for flow cytometric analysis of the spleen. We first ran an exploratory unbiased clustering analysis, using custom code. Of the leukocyte clusters observed in the spleen, two were predominantly derived from CD11c$^{\Delta MHCII}$ cells, one cluster consisting of a neutrophil population (CD11b^{+}GR1^{high}) and one cluster with myeloid precursor cells (CD11b+ Gr1^{int} CD11c^{-} Ly6C^{high} F4/80^{low}) (**Figure 2A**). To investigate the kinetics of these population differences, a conventional flow cytometry analysis approach was used. A massive, progressive expansion of splenic CD11b^{+}GR1^{high} neutrophils was observed in CD11c$^{\Delta MHCII}$ mice as early as 12 weeks (**Figure 2B-C**). Confirming the results of the clustering analysis, the cells comprising the neutrophilic expansion skewed towards immature phenotypes, as there was a significantly higher proportion of neutrophil precursor cells, indicating disordered myeloid hematopoiesis (**Figure 2D-E**). To establish the presence of extramedullary hematopoiesis, we measured the number of splenic stem cells (Lin^{-} CD11b^{-} Sca1^{+} cKit^{+}) and found a significant increase in CD11c$^{\Delta MHCII}$ mice compared to wildtype mice (**Fig 2F-G**). Taken together, these results demonstrate that CD11c$^{\Delta MHCII}$ mice reproduce the MPD phenotype observed with DC numerical deficiency, indicating that functional DC defects, rather than a lack of DCs in a specific differentiation niche, lead to myeloproliferative disease.

Studies on the relationship between DCs and MPD, both previous[11,12] and here, have relied on CD11c-Cre to drive a DC-dependent phenotype. We investigated the degree to which CD11c-Cre gives faithful Cre expression, and found leakage of CD11c-Cre expression in non-DC lineages, including variable penetrance in B cells and macrophages (**Figure S5**). No correlation was observed between the degree of penetrance in non-DC lineages and the manifestation of MPD-like phenotypes (**Figure S5**). Likewise, due to the potential off-target toxicity of Cre [11,12], we compared the phenotype of CD11c-Cre control mice, without homozygous MHCII flox.

These mice did not develop the MPD-like phenotype of CD11c$^{\Delta MHCII}$ mice (**Figure S6**). The DC-restricted recombination activity of CD11c-Cre thus accounts for the observed phenotype.

Myeloproliferative disease results from dysregulated communication between DCs and CD4 T cells

The development of MPD in CD11c$^{\Delta MHCII}$ mice suggested a role for DC-CD4 T cell interaction in restraining neutrophil proliferation. As MHCII on DCs plays a critical role in both CD4$^+$ T cell differentiation in the thymus and CD4$^+$ T cell maintenance and function in the periphery, we profiled the T cell compartment of CD11c$^{\Delta MHCII}$ mice. The absence of MHCII on CD11c$^+$ cells had little impact on double negative thymocytes, double positive thymocytes or single positive (SP) CD8$^+$ T cells (**Figure 3A**). However, consistent with the known role of DCs in negative selection in the thymus [33], the percentage of SP CD4$^+$ T cells was increased in CD11c$^{\Delta MHCII}$ mice (**Figure 3A**). Within the SP CD4$^+$ thymocyte compartment, there was a lower percentage of FoxP3+ cells, but given the increase in total SP CD4$^+$s, the total number of T_{regs} was unchanged (**Figure 3A**). These results are consistent with the established role of CD11c$^+$ DCs in the thymus.

We next investigated the peripheral T cell compartment. Despite the increase in SP CD4$^+$ thymocytes, we observed decreased percentages (**Figure 3B**) and absolute numbers (**Figure S7**) of CD4$^+$ T cells in the periphery of CD11c$^{\Delta MHCII}$ mice. The composition of the CD4$^+$ T cell compartment was strongly impacted by the lack of MHCII on DCs, with significantly greater percentages of naïve CD4$^+$ T cells at 12 weeks of age in CD11c$^{\Delta MHCII}$ mice (**Figure 3C**). The activated CD4$^+$ T cell compartment was smaller in CD11c$^{\Delta MHCII}$ mice, with intact distribution of helper T cell subsets within this smaller compartment, apart from a reduction in IL-2 production by CD4$^+$ T cells (**Figure S8**). This result is consistent with defective antigen priming, where

$CD4^+$ T cells in $CD11c^{\Delta MHCII}$ mice fail to encounter antigen and remain naïve. $Foxp3^+$ regulatory T cells (T_{reg} cells) are also agonist-expanded through MHCII in the periphery, and demonstrated a profound decrease throughout the lifespan of $CD11c^{\Delta MHCII}$ mice (**Figure 3D**). Notably, while the increase in naïve $CD4^+$ T cells became less pronounced over time, indicating a DC-independent source of $CD4^+$ T cell activation, the same was not observed with T_{reg} cells (**Figure 3C-D**), either indicating a more essential role for MHCII on DCs in T_{reg} maintenance than conventional $CD4^+$ T cell activation, or a compounding effect from reduced IL2 production (**Figure S8**). Loss of MHCII on DCs therefore sets up an opposing tension, with a limitation on opportunities for $CD4^+$ T cells to encounter cognate antigen, but also reduced T_{reg} cell numbers contributing to T cell activation. A potential outlet of this tension is the $CD8^+$ T cell population. While there were only small changes in the total $CD8^+$ T cell population in $CD11c^{\Delta MHCII}$ mice (**Figure 3E**), profound activation of $CD8^+$ T cells was observed, with a substantial progressive increase in effector $CD8^+$ cells across time points (**Figure 3F**). This result represents a loss of a T cell control mechanism in $CD11c^{\Delta MHCII}$ mice, providing a potential mechanistic avenue for the observed MPD.

The failure of a T cell checkpoint in $CD11c^{\Delta MHCII}$ mice provides an alternative to the discarded "empty niche" model for MPD development. To test this hypothesis, we crossed $CD11c^{\Delta MHCII}$ mice with Rag^{KO} mice, which lack both T and B cells. Remarkably, none of these mice developed signs of MPD. While $CD11c^{\Delta MHCII}$ mice developed splenomegaly, no $Rag^{KO}CD11c^{\Delta MHCII}$ mice did (**Figure 4A**). To control for the small spleens normally observed in Rag^{KO} mice, we also determined the ratio of spleen weight to total body weight, and again found no difference between $Rag^{KO}CD11c^{\Delta MHCII}$ mice and either wildtype or Rag^{KO} mice (**Figure 4B**). Likewise, we measured the absolute number of splenic neutrophils (**Figure 4C**) and myeloid precursors (**Figure 4D**) and found no increase in $Rag^{KO}CD11c^{\Delta MHCII}$ mice compared to controls, unlike $CD11c^{\Delta MHCII}$ mice. Furthermore, while $CD11c^{\Delta MHCII}$ developed a granulocytic expansion in

the bone-marrow (**Figure 4E**), this phenotype was not observed in *Rag*^{KO}CD11c$^{\Delta MHCII}$ mice. Therefore, lymphocytes are necessary for the development of MPD in settings of DC deficiency.

Having established an unexpected role for the adaptive immune system in driving MPD in CD11c$^{\Delta MHCII}$ mice, we next sought to clarify which cell subset was responsible for this phenomenon. The observed increase in effector CD8^{+} T cells in CD11c$^{\Delta MHCII}$ raised the possibility of a mechanistic pathway whereby reduced T_{reg} cell expansion allowed elevated CD8^{+} T cell activation, driving the MPD. To investigate this possibility, we crossed CD11c$^{\Delta MHCII}$ mice with a β2 microglobulin KO strain, which lack CD8^{+} T cells, creating *β2m*^{KO}CD11c$^{\Delta MHCII}$ mice. Contrary to our hypothesis that CD8^{+} T cells were the downstream cause of MPD in CD11c$^{\Delta MHCII}$ mice, *β2m*^{KO}CD11c$^{\Delta MHCII}$ mice developed myeloproliferation, resembling the disease in CD11c$^{\Delta MHCII}$ mice. We observed a similar degree of splenomegaly in *β2m*^{KO}CD11c$^{\Delta MHCII}$ mice compared to CD11c$^{\Delta MHCII}$ mice (**Figure 5A**), as well as similar percentage (**Figure 5B**) and absolute number (**Figure 5C**) of splenic neutrophils. Moreover, an expansion of neutrophil precursors was identified in the spleen (**Figure 5D**). As CD8 deficiency in CD11c$^{\Delta MHCII}$ mice (i.e., *β2m*^{KO}CD11c$^{\Delta MHCII}$ mice) does not abolish disease, MPD is independent of CD8+ T cells.

The demonstrated lymphocyte-dependency of MPD-like symptoms in CD11c$^{\Delta MHCII}$ mice implicates CD4^{+} T cells as a necessary co-factor in disease development. While CD11c$^{\Delta MHCII}$ mice lack MHCII on DCs, *MHCII*^{KO} mice lack MHCII globally. *MHCII*^{KO} mice therefore combine both a deficiency in MHCII on DCs with a lack of CD4^{+} T cells, owing to the requirement for MHCII on thymic epithelial cells during differentiation. Analysis of MHCII^{KO} mice demonstrates that these mice fail to manifest any of the identified MPD-like phenotypes, with no increase in spleen weight (**Figure 6A**), no increase in splenic neutrophils (**Figure 6B,C**) and no increase in splenic neutrophil precursors (**Figure 6D**). These results suggested that MPD could be

generated through an activatory signal originating from $CD4^+$ T cells, which is normally suppressed by antigen-exposure from DCs, i.e., a signal derived from naïve $CD4^+$ T cells. As MPD in the context of DC numerical deficiency has been attributed to excess Flt3 ligand [11], we measured the expression of Flt3 ligand by naïve and activated CD4+ T cells, in wildtype and $CD11c^{\Delta MHCII}$ mice. Naïve $CD4^+$ T cells from both strains exhibit higher levels of Flt3 ligand expression than antigen-experienced CD4+ T cells (**Figure 6E**). Together these data present a potential molecular model linking MPD to DC:$CD4^+$ T cell interaction, whereby MHCII-TCR interaction is required to quench excessive production of Flt3 ligand by $CD4^+$ T cells.

Discussion

MPD is an unexpected clinical manifestation associated with DC deficiency in both mice [8,11,13–16] and humans [7,18,19]. While a direct link between the DC deficiency and the MPD manifestations is generally accepted, it should be noted that both the mouse models and the human diseases have immunological disturbances beyond that of DCs. In the case of the mouse models, the original systems relied on transgenes driven by the CD11c promoter [11,12]. While often considered “DC specific”, the CD11c promoter is also active in subsets of B cells and macrophages (as observed here). Follow-up publications used alternative promoters, including Tak1 [15] and Zbtb46 [16], which each have their own limitations. Caution is thus warranted when concluding a singular role for DCs in any of these models. Existing evidence, though, strongly implicates DCs as the responsible cell type. In addition to the multiple concordant models showing parallel phenotypes, the reported MPD is not readily explained by off-target effects in other cell types. To our knowledge, no similar phenotypes have been reported with macrophage depletion using liposomal clodronate, CD11b-DTR or lysM-Cre-DTR, nor has MPD been reported in any of the numerous B cell depletion or knockout studies. Likewise, in patients, while IRF8 and GATA2 patients have a deficiency in DCs, the mutations also have pleiotropic effects

throughout the immune system, including in the B cell and macrophage compartments. As DCs are the unifying population altered across these various models and patients, the parsimonious model is to consider MPD to be driven by deficiency in the DC subset, with a formal acknowledgement that the key population is, rather, a GATA2-dependent IRF8-dependent CD11c+ antigen presenting cell.

Given the main physiological role of DCs as professional antigen presenting cells to T cells, a direct biological link between DC deficiency and MPD was not obvious. The main model to explain this phenomenon instead focused on a putative developmental feedback loop in which DC deficiency is sensed, leads to feed back into the haematopoietic stem cell niche, and amplifies differentiation into myeloid precursor cells [11]. A key candidate for this sensing was Flt3-ligand, which is elevated in the serum of CD11c-DTA [11] and TAK1 deficient mice [15], potentially because DCs represent a “ligand sink” due to expression of high levels of Flt3 [34]. Under this model, the loss of DCs would drive MPD either directly, such as the proposal that excess Flt3-ligand drives proliferation of the myeloid precursor cells [11], or via upstream effects, with stem cells responding to the deficiency and being driven into the myeloid precursor lineage, but arresting prior to becoming mature DCs due to genetic blockade. In both cases, however, the linchpin of the model was the numerical deficiency of DCs.

In the current study, we challenged these existing models of MPD in DC deficiency by generating a mouse model where DCs were numerically normal but functionally impaired due to a lack of MHCII. Under the standard developmental feedback models, such a system should allow the autoimmune manifestations of DC-deficiency [12] but would not manifest in MPD. Instead, we observed extramedullary haematopoiesis and large myeloid-lineage proliferation, with neutrophilia and myeloid precursors driving splenomegaly. This data demonstrates that either numerical DC deficiency a loss of DC-dependent functions is capable of driving MPD,

with parsimony suggesting the latter effect as a disease driver in both cases. With the only functional impairment induced being a lack of antigen presentation via MHCII, this data demonstrates that the collaboration between DC and $CD4^+$ T cells is at the heart of myeloproliferative control. The combination of phenotypic correction with additional Rag-deficiency and disease progression with β2m-deficiency suggests that $CD4^+$ T cells need to be present to drive disease. This is further supported by the suppression of MPD manifestations in MHCII-deficient mice, which recapitulate the functional deficiency of $CD11c^{\Delta MHCII}$ mice (i.e., DCs are MHCII-deficient) but additionally have an almost complete absence of peripheral $CD4^+$ T cells, due to developmental blockade in the thymus. A viable model to explain these data requires both: a) the presence of an activating signal originating from a subset of $CD4^+$ T cells; and b) a suppressive signal originating from DCs which quenches this activating signal. The simplest model integrating these key features that is compatible with the phenotyping data above is one where naïve CD4+ T cells express the activating signal until MHCII-mediated antigen experience. The effect may also be mediated in part by loss of an inhibitory signal conferred by $CD4^+$ T cells, such as the deficit in T_{reg} cells, however an activating signal needs to be part of the model, otherwise other mouse strains of $CD4^+$ T cell deficiency would exhibit MPD in the presence of normal DC number and function. While it is perplexing that an activating signal comes from a compartment characterized here as predominantly naïve, it should be noted that some stimulatory ligands are expressed at higher levels by naïve $CD4^+$ T cells and go down with antigen experience. Here we demonstrate that Flt3 ligand is one such signal. While a previous study [35] reported no difference in Flt3L production between naïve and memory CD4+ T cells, both our study and the publically available database Immgen support a two-fold increase in expression in naïve CD4+ T cells. Indeed naïve CD4+ T cells are the highest haematopoetic source for Flt3 ligand in both mouse and human (www.immgen.org). With the Flt3-Flt3 ligand axis key to myeloid proliferation, this model potentially unifies the cellular and

molecular mechanisms linking DC deficiency to MPD.

The identification of DC-CD4$^+$ T cell communication defects as a driver for MPD brings up the potential intersection of MPD and autoimmunity. Antigen presentation by DCs is important for the negative selection of autoreactive T cells [2–4], although the degree has been debated given the overlapping functionality of medullary thymic epithelial cells [36–38]. Defects in tolerance processes brought about by DC deficiency could thus be reasonably expected to drive T cell-dependent autoimmunity, although this would also be countered by the opposing loss of T cell priming by DCs. One of the initial reports of murine DC-deficiency observed severe autoimmune pathology [12], which could, in principle, have driven secondary MPD. Conversely, both our study here and other published models [11] found no sign of either autoimmune disease, or, indeed, any overt CD4$^+$ T cell activation. A reconciliation of these findings may be found in the identification of a key role of the microbiota in the inflammatory aspects of disease [39]. Thus the presence or absence of autoimmunity across the different studies could potentially be explained by differences in colony microflora. Notably, while this study took a similar functional-deficiency approach to our study, the confounding inflammation and the limit of monitoring to 14 weeks in most experiments precluded the conclusions made here. While we do not exclude a potential amplification of MPD by autoimmune or inflammatory processes, these processes are not necessary for MPD. Instead, the MPD driven by DC deficiency represents a novel DC-CD4$^+$ T cell communication failure, independent of the tolerance defects described.

The model of MPD developed here has implications for human disease. The link between DC deficiency and MPD is not limited to mouse models; patients with GATA2 and IRF8 mutations also manifest both DC deficiency and myeloproliferative and myelodysplastic disorders[7,17–19]. Under the “open niche” model originally proposed to explain this link, treatment of MPD requires filling the empty DC niche, which can currently only be performed through bone-marrow

transplantation. If our two-step model is correct, with naïve $CD4^+$ T cells providing an activatory signal and DCs providing a quencher, a second potential intervention point opens up: the naïve $CD4^+$ T cell. If this model is validated in patients, then therapeutic intervention that reduces the production of the activatory signal (likely, Flt3 ligand) from naïve $CD4^+$ T cell would reduce the development of myeloproliferative disorders.

Acknowledgements

This work was supported by the FWO and the VIB Grand Challenges program. SH-B is an FWO fellow. JB is a fellow of the Belgian-American Educational Foundation. The authors have declared that no conflict of interest exists.

Author contributions

SHB, JSB and AL ran the experiments. SHB, JSB and CR analyzed data. PK contributed vital reagents. SHB and A Liston designed the study. SHB, JSB and A Liston wrote the manuscript.

References

1. Boscardin SB, Hafalla JCR, Masilamani RF, et al. Antigen targeting to dendritic cells elicits long-lived T cell help for antibody responses. *J Exp Med*. 2006;203(3):599-606. doi:10.1084/jem.20051639
2. Bonasio R, Scimone ML, Schaerli P, Grabie N, Lichtman AH, von Andrian UH. Clonal deletion of thymocytes by circulating dendritic cells homing to the thymus. *Nat Immunol*. 2006;7(10):1092-1100. doi:10.1038/ni1385
3. Proietto AI, van Dommelen S, Zhou P, et al. Dendritic cells in the thymus contribute to T-regulatory cell induction. *Proc Natl Acad Sci*. 2008;105(50):19869-19874. doi:10.1073/pnas.0810268105
4. Gallegos AM, Bevan MJ. Central Tolerance to Tissue-specific Antigens Mediated by Direct and Indirect Antigen Presentation. *J Exp Med*. 2004;200(8):1039-1049. doi:10.1084/jem.20041457
5. Mahnke K, Qian Y, Knop J, Enk AH. Induction of CD4+/CD25+ regulatory T cells by targeting of antigens to immature dendritic cells. *Blood*. 2003;101(12):4862-4869. doi:10.1182/blood-2002-10-3229

6. Jung S, Unutmaz D, Wong P, et al. In vivo depletion of CD11c+ dendritic cells abrogates priming of CD8+ T cells by exogenous cell-associated antigens. *Immunity*. 2002;17(2):211-220. doi:10.1016/S1074-7613(02)00365-5
7. Hambleton S, Salem S, Bustamante J, et al. *IRF8* Mutations and Human Dendritic-Cell Immunodeficiency. *N Engl J Med*. 2011;365(2):127-138. doi:10.1056/NEJMoa1100066
8. Satpathy AT, Briseño CG, Cai X, et al. Runx1 and Cbfβ regulate the development of Flt3^{+} dendritic cell progenitors and restrict myeloproliferative disorder. *Blood*. 2014;123(19):2968-2977. doi:10.1182/blood-2013-11-539643
9. Kassim SH, Rajasagi NK, Zhao X, Chervenak R, Jennings SR. In Vivo Ablation of CD11c-Positive Dendritic Cells Increases Susceptibility to Herpes Simplex Virus Type 1 Infection and Diminishes NK and T-Cell Responses. *J Virol*. 2006;80(8):3985-3993. doi:10.1128/JVI.80.8.3985-3993.2006
10. Fukaya T, Murakami R, Takagi H, et al. Conditional ablation of CD205+ conventional dendritic cells impacts the regulation of T-cell immunity and homeostasis in vivo. *Proc Natl Acad Sci*. 2012;109(28):11288-11293. doi:10.1073/pnas.1202208109
11. Birnberg T, Bar-On L, Sapoznikov A, et al. Lack of Conventional Dendritic Cells Is Compatible with Normal Development and T Cell Homeostasis, but Causes Myeloid Proliferative Syndrome. *Immunity*. 2008;29(6):986-997. doi:10.1016/j.immuni.2008.10.012
12. Ohnmacht C, Pullner A, King SBS, et al. Constitutive ablation of dendritic cells breaks self-tolerance of CD4 T cells and results in spontaneous fatal autoimmunity. *J Exp Med*. 2009;206(3):549-559. doi:10.1084/jem.20082394
13. Holtschke T, Löhler J, Kanno Y, et al. Immunodeficiency and chronic myelogenous leukemia-like syndrome in mice with a targeted mutation of the ICSBP gene. *Cell*. 1996;87(2):307-317. doi:10.1016/S0092-8674(00)81348-3
14. Turcotte K, Gauthier S, Tuite A, Mullick A, Malo D, Gros P. A mutation in the Icsbp1 gene causes susceptibility to infection and a chronic myeloid leukemia-like syndrome in BXH-2 mice. *J Exp Med*. 2005;201(6):881-890. doi:10.1084/jem.20042170
15. Wang Y, Huang G, Vogel P, Neale G, Reizis B, Chi H. Transforming growth factor beta-activated kinase 1 (TAK1)-dependent checkpoint in the survival of dendritic cells promotes immune homeostasis and function. *Proc Natl Acad Sci*. 2012;109(6):E343-E352. doi:10.1073/pnas.1115635109
16. Meredith MM, Liu K, Darrasse-Jeze G, et al. Expression of the zinc finger transcription factor zDC (Zbtb46, Btbd4) defines the classical dendritic cell lineage. *J Exp Med*. 2012;209(6):1153-1165. doi:10.1084/jem.20112675
17. Bigley V, Maisuria S, Cytlak U, et al. Biallelic interferon regulatory factor 8 mutation: A complex immunodeficiency syndrome with dendritic cell deficiency, monocytopenia, and immune dysregulation. *J Allergy Clin Immunol*. November 2017. doi:10.1016/j.jaci.2017.08.044
18. Hahn CN, Chong C-E, Carmichael CL, et al. Heritable GATA2 mutations associated with familial myelodysplastic syndrome and acute myeloid leukemia. *Nat Genet*. 2011;43(10):1012-1017. doi:10.1038/ng.913
19. Hsu AP, Sampaio EP, Khan J, et al. Mutations in GATA2 are associated with the autosomal dominant and sporadic monocytopenia and mycobacterial infection (MonoMAC) syndrome. *Blood*. 2011;118(10):2653-2655. doi:10.1182/blood-2011-05-356352
20. Caton ML, Smith-Raska MR, Reizis B. Notch-RBP-J signaling controls the homeostasis of CD8- dendritic cells in the spleen. *J Exp Med*. 2007;204(7):1653-1664. doi:10.1084/jem.20062648
21. Hashimoto K, Joshi SK, Koni PA. A conditional null allele of the major histocompatibility IA-beta chain gene. *Genesis*. 2002;32(2):152-153.

http://www.ncbi.nlm.nih.gov/pubmed/11857806. Accessed May 9, 2018.
22. Hao Z, Rajewsky K. Homeostasis of peripheral B cells in the absence of B cell influx from the bone marrow. *J Exp Med*. 2001;194(8):1151-1164. http://www.ncbi.nlm.nih.gov/pubmed/11602643. Accessed May 9, 2018.
23. Koller BH, Marrack P, Kappler JW, Smithies O. Normal development of mice deficient in beta 2M, MHC class I proteins, and CD8+ T cells. *Science*. 1990;248(4960):1227-1230. http://www.ncbi.nlm.nih.gov/pubmed/2112266. Accessed May 9, 2018.
24. Cosgrove D, Gray D, Dierich a, et al. Mice lacking MHC class II molecules. *Cell*. 1991;66(5):1051-1066. doi:10.1016/0092-8674(91)90448-8
25. R Core Team. R Foundation for Statistical Computing. 2014:URL https://www.R-project.org/. http://www.r-project.org/.
26. Finak G JM. flowWorkspace: Infrastructure for representing and interacting with the gated cytometry. 2011:R package version 3.26.9.
27. Van Gassen S, Callebaut B, Van Helden MJ, et al. FlowSOM: Using self-organizing maps for visualization and interpretation of cytometry data. *Cytom Part A*. 2015;87(7):636-645. doi:10.1002/cyto.a.22625
28. Van Der Maaten LJP, Hinton GE. Visualizing high-dimensional data using t-sne. *J Mach Learn Res*. 2008;9:2579-2605. doi:10.1007/s10479-011-0841-3
29. Krijthe J. Rtsne: T-Distributed Stochastic Neighbor Embedding using Barnes-Hut Implementation. *R Packag version 010, URL http//CRAN R-project org/package= Rtsne*. 2015:URL https://github.com/jkrijthe/Rtsne. R package v.
30. Wickham H. ggplot2: Elegant Graphics for Data Analysis. 2009:URL http://ggplot2.org.
31. Neuwirth E. RColorBrewer: ColorBrewer palettes. *R Packag version 11-2*. 2014:https://cran.R-project.org/package=RColorBrewer. doi:citeulike-article-id:5433478
32. Shi J, Petrie HT. Activation Kinetics and Off-Target Effects of Thymus-Initiated Cre Transgenes. *PLoS One*. 2012. doi:10.1371/journal.pone.0046590
33. Audiger C, Rahman MJ, Yun TJ, Tarbell K V., Lesage S. The Importance of Dendritic Cells in Maintaining Immune Tolerance. *J Immunol*. 2017;198(6):2223-2231. doi:10.4049/jimmunol.1601629
34. Waskow C, Liu K, Darrasse-Jèze G, et al. The receptor tyrosine kinase Flt3 is required for dendritic cell development in peripheral lymphoid tissues. *Nat Immunol*. 2008;9(6):676-683. doi:10.1038/ni.1615
35. Saito Y, Boddupalli CS, Borsotti C, Manz MG. Dendritic cell homeostasis is maintained by nonhematopoietic and T-cell-produced Flt3-ligand in steady state and during immune responses. *Eur J Immunol*. 2013;43(6):1651-1658. doi:10.1002/eji.201243163
36. Aschenbrenner K, D'Cruz LM, Vollmann EH, et al. Selection of Foxp3+ regulatory T cells specific for self antigen expressed and presented by Aire+ medullary thymic epithelial cells. *Nat Immunol*. 2007;8(4):351-358. doi:10.1038/ni1444
37. Hinterberger M, Aichinger M, da Costa OP, Voehringer D, Hoffmann R, Klein L. Autonomous role of medullary thymic epithelial cells in central CD4+ T cell tolerance. *Nat Immunol*. 2010;11(6):512-519. doi:10.1038/ni.1874
38. Perry JSA, Lio CWJ, Kau AL, et al. Distinct contributions of Aire and antigen-presenting-cell subsets to the generation of self-tolerance in the thymus. *Immunity*. 2014;41(3):414-426. doi:10.1016/j.immuni.2014.08.007
39. Loschko J, Schreiber HA, Rieke GJ, et al. Absence of MHC class II on cDCs results in microbial-dependent intestinal inflammation. *J Exp Med*. 2016;213(4):517-534. doi:10.1084/jem.20160062

Figure legends

Figure 1. Dendritic cell functional impairment drives myeloproliferative disease. Wildtype and CD11c$^{\Delta MHCII}$ mice were assessed by flow cytometry at 12 weeks, 20 weeks, 30 weeks and one year of age. **(A)** Representative histogram of MHCII in splenic CD11c+ cells in wildtype and CD11c$^{\Delta MHCII}$. **(B)** Percentage of cDCs at 12 weeks (n=11,13), 20 weeks (n=22,16), 30 weeks (n=18,14) and one year (n=22,25) of age and **(C)** pDCs in wildtype and CD11c$^{\Delta MHCII}$ mice at 12 weeks (n=6, 11), 20 weeks (=15, 12), 30 weeks (n=3, 3) and one year (n=16, 19) of age . **(D)** Wildtype and CD11c$^{\Delta MHCII}$ mice were assessed for body weight at 12 weeks (n=11, 13), 20 weeks (n=21, 16), 30 weeks (n=19, 13) and one year (n=24, 25) of age and **(E)** spleen weight at 12 weeks (n=11, 13), 20 weeks (n=22, 16), 30 weeks (n=20, 16) and one year (n=23, 25) of age. Dashed line indicates threshold for splenomegaly (two standard deviations above the mean of wildtype mice from all age group). Median and individual data points are shown. **(F)** Cumulative incidence plot of splenomegaly over time in wildtype and CD11c$^{\Delta MHCII}$ mice using a Kaplan-Meier curve (all mice were censored at the time of analysis). Log-rank test used for comparison between curves.

Figure 2. Mixed myeloid composition of myeloproliferative disease in CD11c$^{\Delta MHCII}$ mice. Wildtype and CD11c$^{\Delta MHCII}$ mice were assessed by flow cytometry at 12 weeks, 20 weeks, 30 weeks and one year of age **(A)** tSNE projection of splenocytes of one year old mice stained with myeloid markers (CD11b, Gr1, Ly6C, CD11c and F4/80). Cells are grouped into clusters using FlowSom, with blue representing wildtype splenocytes and red representing CD11c$^{\Delta MHCII}$ splenocytes. Marker composition of the two identified clusters (neutrophils and myeloid precursor-like cells) predominantly populated by CD11c$^{\Delta MHCII}$ splenocytes. **(B)** Absolute number of polymorphonuclear neutrophils (PMN, defined as CD11b^{+}Gr1^{high}) in the spleen at 12 weeks (n=11, 13), 20 weeks (n=22, 16), 30 weeks (n=18, 14) and one year (n=22, 23) of age. The dotted line represents the threshold (two standard deviations above the mean of wildtype mice) of neutropenia. Median and individual data points are shown. **(C)** Cumulative incidence plot for neutrophilia over time in wildtype and CD11c$^{\Delta MHCII}$ mice using Kaplan-Meier curve while all mice were censored at the time of analysis. Log-rank test used for comparison between curves. **(D)** Absolute number of neutrophils-like precursor population in the spleen (defined as CD11b^{+}Gr1^{int}LyC6^{int}CD11c^{-}) in the spleen at 12 weeks (n=9, 11), 20 weeks (n=19, 16), 30 weeks (n=12, 7) and one year (n=22, 23) of age. The dotted line represents the threshold (two standard deviations above the mean of wildtype mice) of increased myeloid precursor-like cells. Median and individual data points are shown. **(E)** Cumulative incidence plot for development of increased myeloid precursor-like over time in wildtype and CD11c$^{\Delta MHCII}$ mice using Kaplan-Meier curve while all mice were censored at the time of analysis. Log-rank test used for comparison between curves. **(F)** Absolute number and **(G)** percentage of splenic haematopoietic stem cells (HSCs, defined as Lin^{-} [TER119, CD3, NK1.1, CD11b, B220] Sca1^{+} cKit^{+}) in the spleen at 12 weeks (n=9, 11), 20 weeks (n=18, 14), 30 weeks (n=8, 4) and one year (n=20, 17) of age. Median and individual data points are shown.

Figure 3. Alterations in the peripheral T cell compartment in CD11c$^{\Delta MHCII}$ mice. Wildtype and CD11c$^{\Delta MHCII}$ mice were assessed by flow cytometry for the T cell compartment at 12 weeks

(n=11, 13), 20 weeks (n=22,16), 30 weeks (n=18, 11) and one year (n=22, 25) of age. **(A)** Percentages of T cell subsets in the thymus at 30 weeks (n=6,7). **(B)** Percentages of total $CD4^+$ T cells among total splenocytes. **(C)** Percentages of naïve $CD4^+$ T cells ($CD4^+CD62L^+CD44^-$) among $CD4^+$ T splenocytes. **(D)** Percentage of Tregs ($CD4^+Foxp3^+$) gated on splenic $CD4^+$ T cells. **(E)** Percentage of $CD8^+$ T cells among total splenocytes. **(F)** Percentage of effector $CD8^+$ T cells ($CD8^+CD62L^-CD44^+$) gated on splenic $CD8^+$ T cells. Median and individual data points are shown.

Figure 4. Rag-deficiency prevents MPD. *Rag*^{KO} and *Rag*^{KO}\CD11c$^{\Delta MHCII}$ mice were assessed by flow cytometry at one year of age. Wildtype and CD11c$^{\Delta MHCII}$ are shown for comparative purposes. **(A)** Spleen weight in milligrams (n=23, 25, 8, 9). Dashed line indicates threshold for splenomegaly (two standard deviations above the mean of wildtype mice from all age group) **(B)** Ratio spleen weight to total weight (n=22, 25, 8, 9) **(C)** Absolute number ($x10^6$) of peripheral mononuclear neutrophils (PMN) ($CD11b^{high}$ $Gr1^+$) among total splenocytes. (n=22, 23, 7, 8). Dashed line indicates threshold for neutrophilia (two standard deviations above the mean of wildtype mice from all age group) **(D)** Absolute number of neutrophil precursor-like population among total splenocytes (n=22, 23, 7, 8)**.** Dashed line indicates threshold for higher neutrophil precursors (two standard deviations above the mean of wildtype mice from all age group) **(E)** The ratio of granulocytes to erythroid cell precursors in the bone marrow (BM) (n=10, 17, 8, 9). Dashed line indicates threshold for higher ratio (two standard deviations above the mean of wildtype mice from all age group). Mean ± SEM and individual data points are shown.

Figure 5. MPD is independent of CD8 T cell activation. β2m^{KO}CD11c$^{\Delta MHCII}$ mice were assessed by flow cytometry. Wildtype and CD11c$^{\Delta MHCII}$ are shown for comparative purposes. (**A)** Spleen weight in milligrams and **(B)** Percentage of peripheral mononuclear neutrophils (PMN) ($CD11b^{high}$ $Gr1^+$) among total splenocytes at 12 weeks (n=11,13,6), 20 weeks (n=22,16,3), 30 weeks (n=22,16,5) and one year (n=23,25,5) of age. **(C)** Absolute number of PMN among total splenocytes at 12 weeks (n=11,13,6), 20 weeks (n=22,16,3), 30 weeks (n=18,14,5) and one year (n=22,23,5) of age. **D)** Absolute number of myeloid precursor-like cells among total splenocytes at 12 weeks (n=11,13,6), 20 weeks (n=22,16,2), 30 weeks (n=12,7,5) and one year (n=22,23,5) of age. Mean ± SEM and individual data points are shown.

Figure 6: MPD development relies on the presence of CD4 T cells. (A-D) MHCII^{KO} mice were assessed by flow cytometry. Wildtype and CD11c$^{\Delta MHCII}$ are shown for comparative purposes. **(A)** Spleen weight in milligrams and **(B)** Percentage of peripheral mononuclear neutrophils (PMN) ($CD11b^{high}$ $Gr1^+$) among total splenocytes at 12 weeks (n=11,13,6), 30 weeks (n=22,16,3) and one year (n=23,25,4) of age. **(C)** Absolute number of PMN among total splenocytes at 12 weeks (n=11,13,6), 30 weeks (n=18,11,3) and one year (n=22,23,4) of age. **(D)** Absolute number of myeloid precursor-like cells among total splenocytes at 12 weeks (n=9,11,6), 30 weeks (n=12,7,3) and one year (n=22,23,4) of age. Mean ± SEM and individual data points are shown. **(E)** Naïve ($CD25^-CD62L^+CD44^-$) and memory ($CD25^-CD44^+$) CD4 cells from 6 mice were sorted and qPCR for Flt3L was performed. Mean ± SEM are shown. p value reported for unpaired t test.

Figure 1

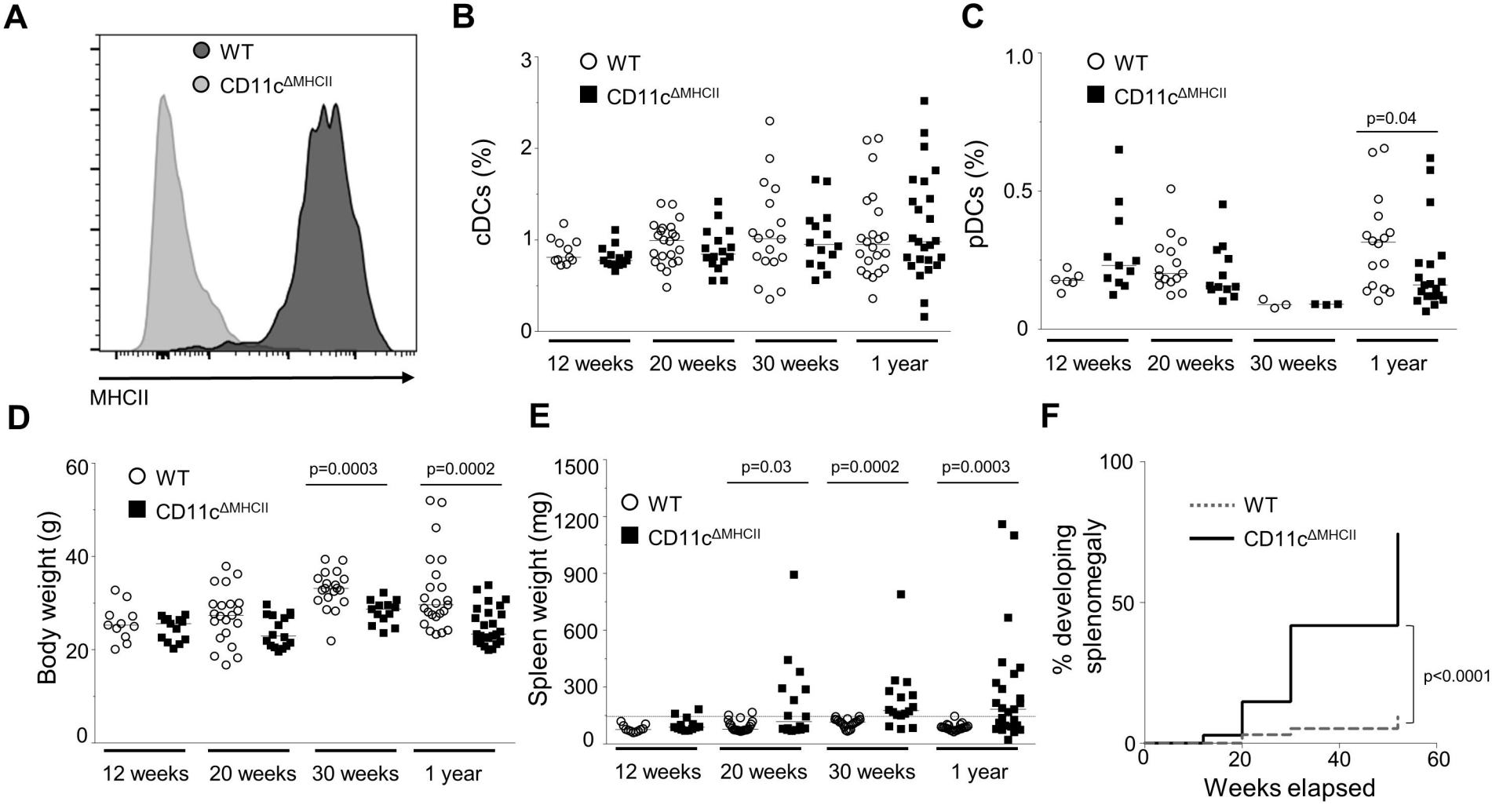
A
WT
CD11c$^{\Delta MHCII}$
MHCII
B
WT
CD11c$^{\Delta MHCII}$
cDCs (%)
12 weeks
20 weeks
30 weeks
1 year
C
WT
CD11c$^{\Delta MHCII}$
pDCs (%)
p=0.04
12 weeks
20 weeks
30 weeks
1 year
D
WT
CD11c$^{\Delta MHCII}$
Body weight (g)
p=0.0003
p=0.0002
12 weeks
20 weeks
30 weeks
1 year
E
WT
CD11c$^{\Delta MHCII}$
Spleen weight (mg)
p=0.03
p=0.0002
p=0.0003
12 weeks
20 weeks
30 weeks
1 year
F
WT
CD11c$^{\Delta MHCII}$
% developing splenomegaly
p<0.0001
Weeks elapsed

Figure 2

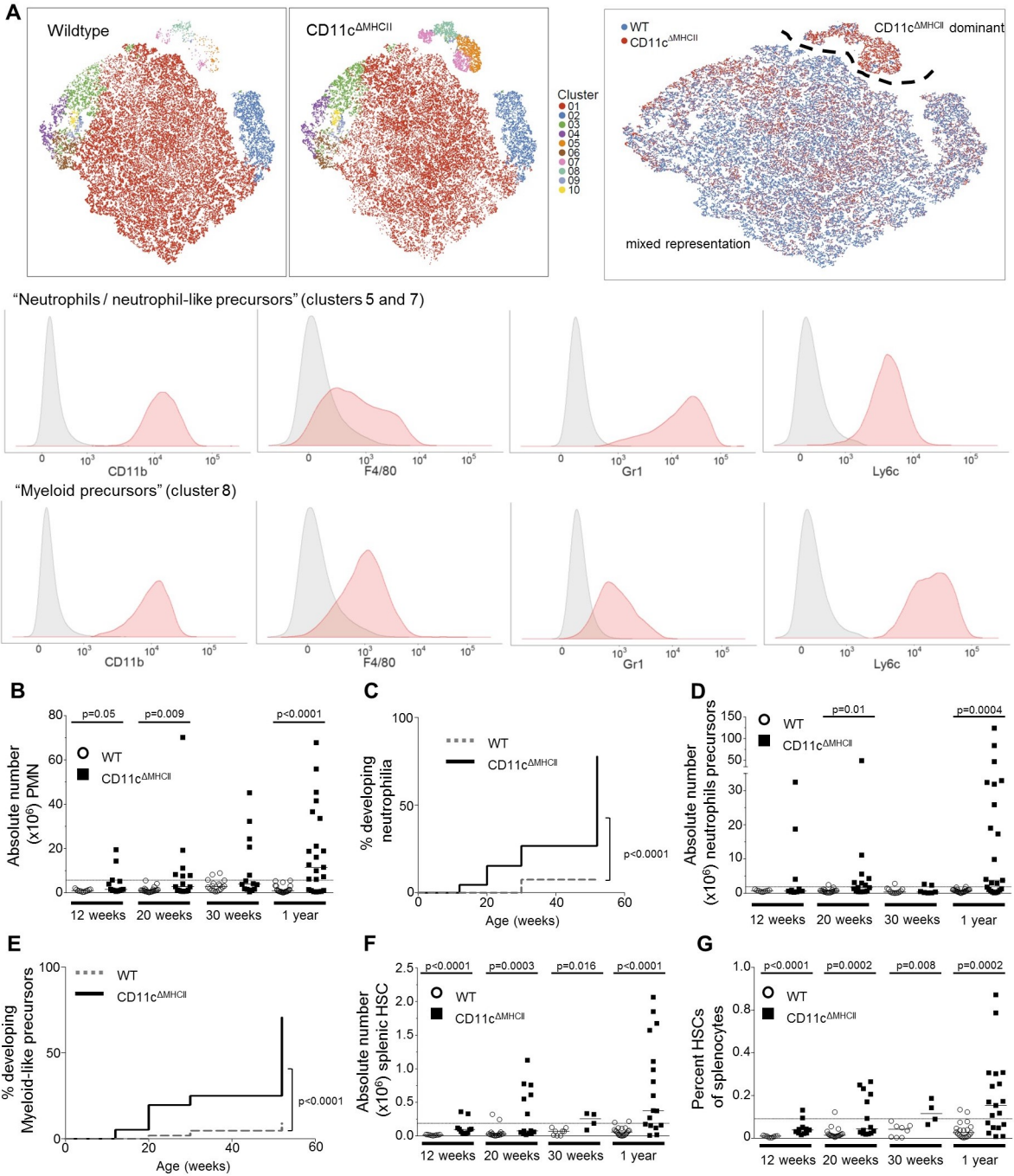
A
Wildtype
CD11c$^{\Delta MHCII}$
Cluster
01
02
03
04
05
06
07
08
09
10
WT
CD11c$^{\Delta MHCII}$
CD11c$^{\Delta MHCII}$ dominant
mixed representation
"Neutrophils / neutrophil-like precursors" (clusters 5 and 7)
CD11b
F4/80
Gr1
Ly6c
"Myeloid precursors" (cluster 8)
CD11b
F4/80
Gr1
Ly6c
B
Absolute number (x10^6) PMN
p=0.05
p=0.009
p<0.0001
WT
CD11c$^{\Delta MHCII}$
12 weeks
20 weeks
30 weeks
1 year
C
% developing neutrophilia
WT
CD11c$^{\Delta MHCII}$
p<0.0001
Age (weeks)
D
Absolute number (x10^6) neutrophils precursors
p=0.01
p=0.0004
WT
CD11c$^{\Delta MHCII}$
12 weeks
20 weeks
30 weeks
1 year
E
% developing Myeloid-like precursors
WT
CD11c$^{\Delta MHCII}$
p<0.0001
Age (weeks)
F
Absolute number (x10^6) splenic HSC
p<0.0001
p=0.0003
p=0.016
p<0.0001
WT
CD11c$^{\Delta MHCII}$
12 weeks
20 weeks
30 weeks
1 year
G
Percent HSCs of splenocytes
p<0.0001
p=0.0002
p=0.008
p=0.0002
WT
CD11c$^{\Delta MHCII}$
12 weeks
20 weeks
30 weeks
1 year

Figure 3

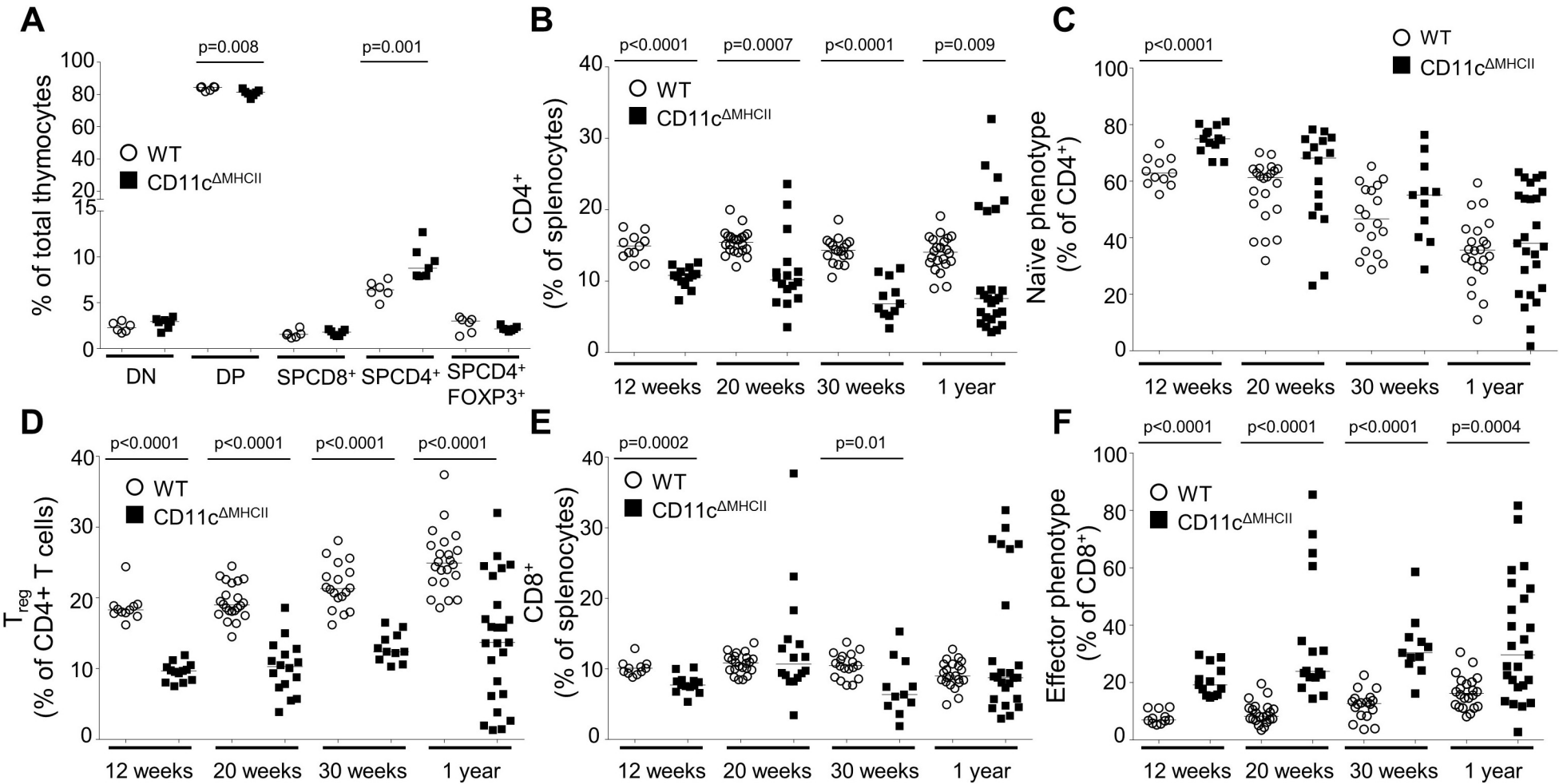
A
% of total thymocytes
p=0.008
p=0.001
WT
CD11c^ΔMHCII
DN
DP
SPCD8+
SPCD4+
SPCD4+ FOXP3+
B
CD4+ (% of splenocytes)
p<0.0001
p=0.0007
p<0.0001
p=0.009
12 weeks
20 weeks
30 weeks
1 year
C
Naïve phenotype (% of CD4+)
p<0.0001
D
Treg (% of CD4+ T cells)
p<0.0001
p<0.0001
p<0.0001
p<0.0001
E
CD8+ (% of splenocytes)
p=0.0002
p=0.01
F
Effector phenotype (% of CD8+)
p<0.0001
p<0.0001
p<0.0001
p=0.0004

Figure 4

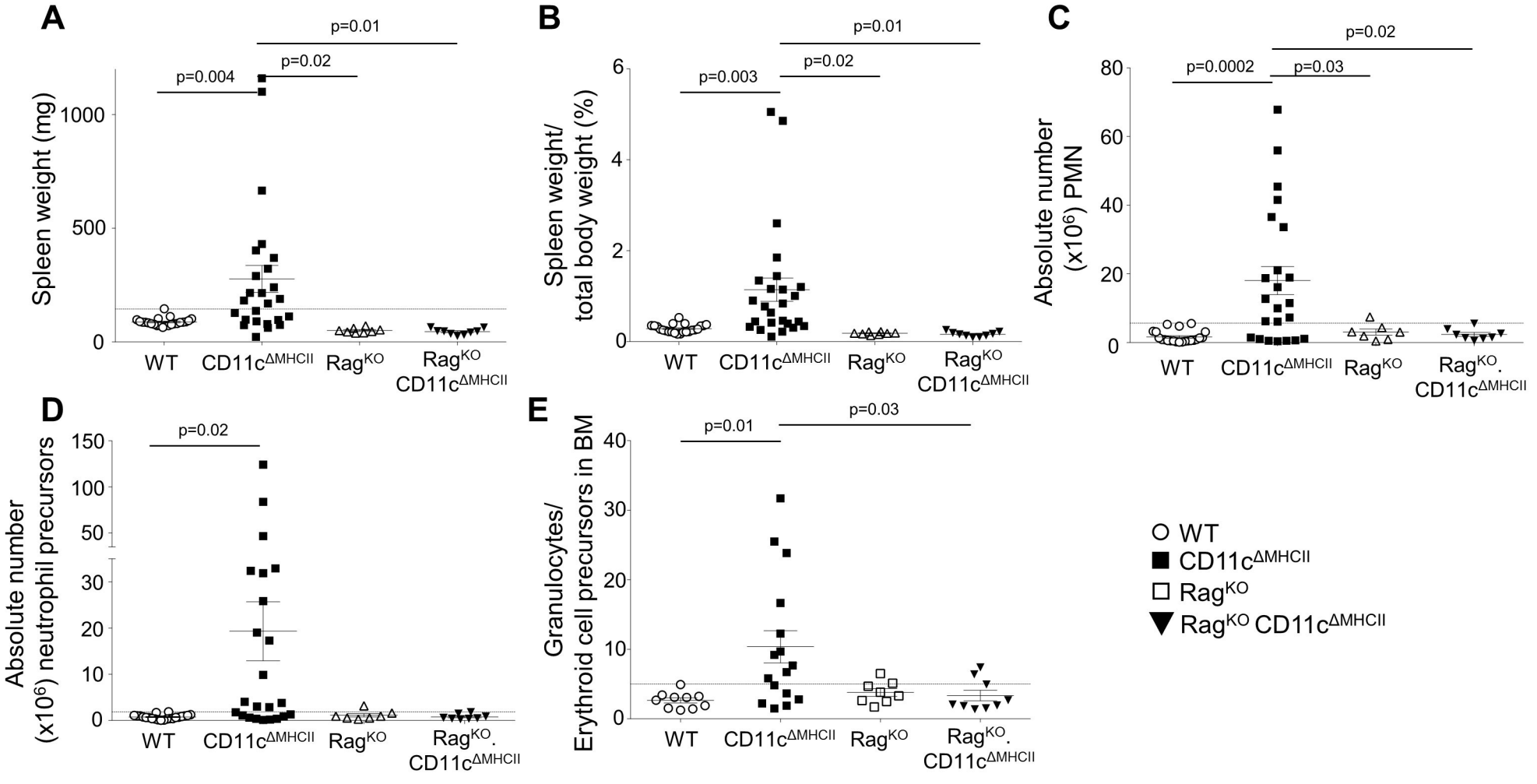
A
p=0.01
p=0.02
p=0.004
Spleen weight (mg)
1000
500
0
WT
CD11c^ΔMHCII
Rag^KO
Rag^KO CD11c^ΔMHCII
B
p=0.01
p=0.02
p=0.003
Spleen weight/ total body weight (%)
6
4
2
0
WT
CD11c^ΔMHCII
Rag^KO
Rag^KO CD11c^ΔMHCII
C
p=0.02
p=0.03
p=0.0002
Absolute number (x10^6) PMN
80
60
40
20
0
WT
CD11c^ΔMHCII
Rag^KO
Rag^KO. CD11c^ΔMHCII
D
p=0.02
Absolute number (x10^6) neutrophil precursors
150
100
50
30
20
10
0
WT
CD11c^ΔMHCII
Rag^KO
Rag^KO. CD11c^ΔMHCII
E
p=0.03
p=0.01
Granulocytes/ Erythroid cell precursors in BM
40
30
20
10
0
WT
CD11c^ΔMHCII
Rag^KO
Rag^KO. CD11c^ΔMHCII
WT
CD11c^ΔMHCII
Rag^KO
Rag^KO CD11c^ΔMHCII

Figure 5

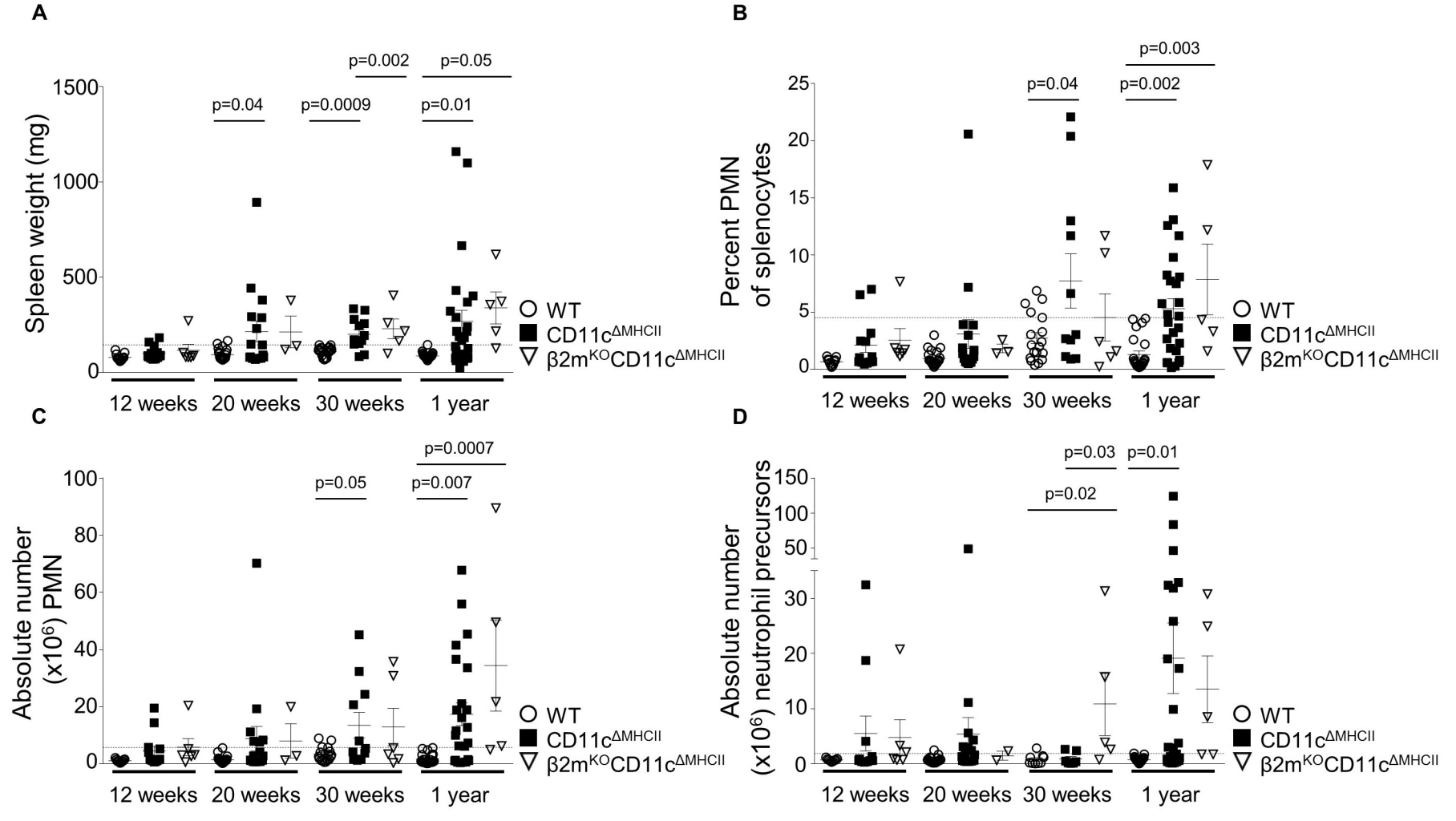
A
Spleen weight (mg)
1500
1000
500
0
p=0.04
p=0.0009
p=0.002
p=0.01
p=0.05
12 weeks
20 weeks
30 weeks
1 year
WT
CD11c$^{\Delta MHCII}$
β2m^{KO}CD11c$^{\Delta MHCII}$
B
Percent PMN of splenocytes
25
20
15
10
5
0
p=0.04
p=0.002
p=0.003
12 weeks
20 weeks
30 weeks
1 year
WT
CD11c$^{\Delta MHCII}$
β2m^{KO}CD11c$^{\Delta MHCII}$
C
Absolute number (x10^6) PMN
100
80
60
40
20
0
p=0.05
p=0.007
p=0.0007
12 weeks
20 weeks
30 weeks
1 year
WT
CD11c$^{\Delta MHCII}$
β2m^{KO}CD11c$^{\Delta MHCII}$
D
Absolute number (x10^6) neutrophil precursors
150
100
50
30
20
10
0
p=0.02
p=0.03
p=0.01
12 weeks
20 weeks
30 weeks
1 year
WT
CD11c$^{\Delta MHCII}$
β2m^{KO}CD11c$^{\Delta MHCII}$

Figure 6

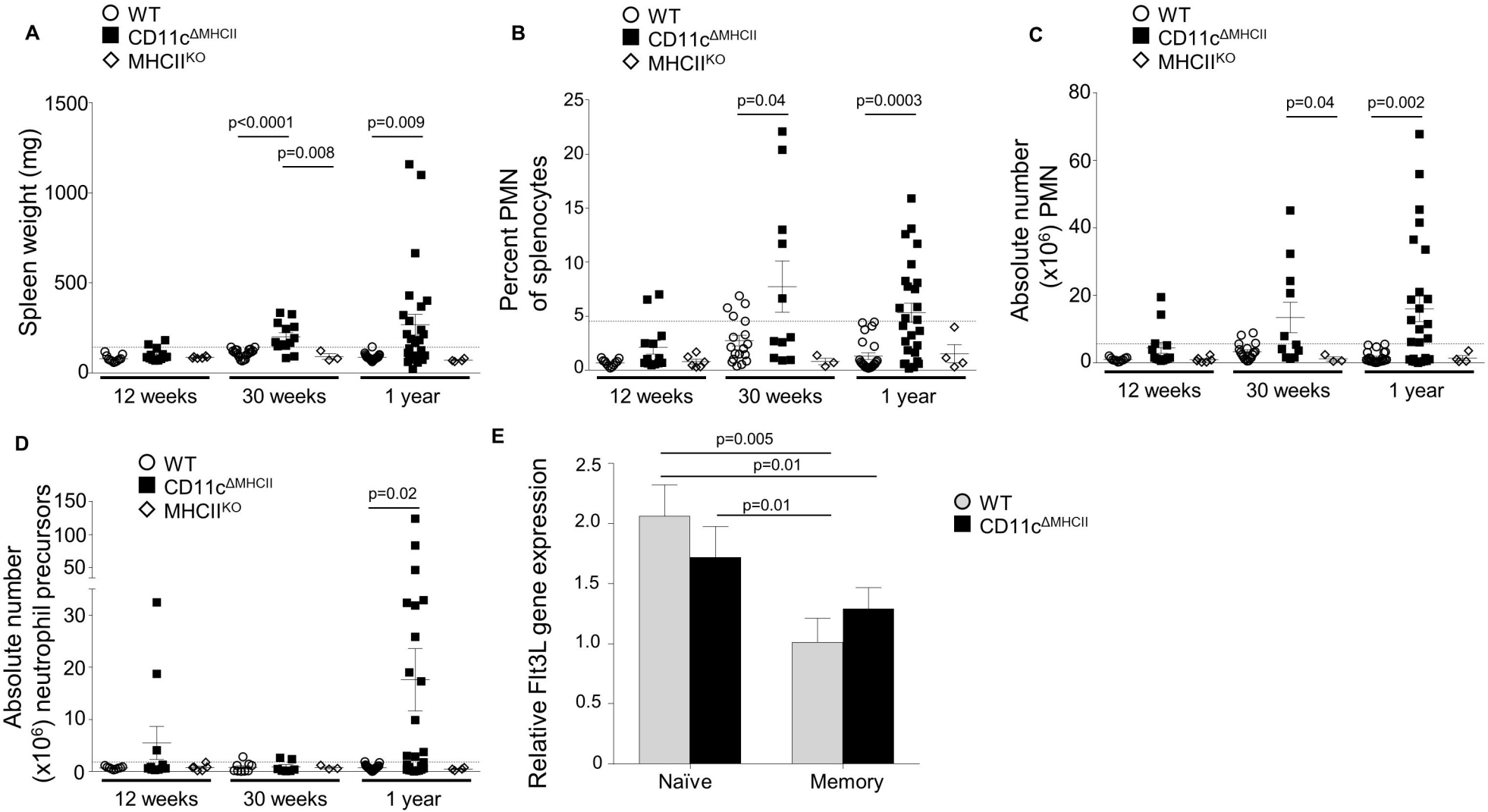
A
WT
CD11c^ΔMHCII
MHCII^KO
Spleen weight (mg)
1500
1000
500
0
p<0.0001
p=0.008
p=0.009
12 weeks
30 weeks
1 year
B
Percent PMN of splenocytes
25
20
15
10
5
0
p=0.04
p=0.0003
C
Absolute number (x10^6) PMN
80
60
40
20
0
p=0.04
p=0.002
D
Absolute number (x10^6) neutrophil precursors
150
100
50
30
20
10
p=0.02
E
Relative Flt3L gene expression
2.5
2.0
1.5
1.0
0.5
p=0.005
p=0.01
p=0.01
Naïve
Memory

Prepublished online October 17, 2018;
doi:10.1182/blood-2018-05-850321

Murine myeloproliferative disorder as a consequence of impaired collaboration between dendritic cells and CD4 T cells

Stéphanie Humblet-Baron, John S. Barber, Carlos Roca, Aurelie Lenaerts, Pandelakis A. Koni and Adrian Liston